Field-dependent carrier decay dynamics in strained $In_xGa_{1-x}N/GaN$ quantum wells

Y. D. Jho, J. S. Yahng, E. Oh,* and D. S. Kim
Department of Physics, Seoul National University, Seoul 151-747, Korea
(Received 21 November 2001; published 31 July 2002)

We have studied the effects of an external electric field on photoluminescence spectra and carrier lifetimes in strained $In_xGa_{1-x}N/GaN$ quantum wells embedded in *p-i-n* light-emitting diode (LED) structures. Two sample structures with $x=0.15$ for blue LED's and 0.2 for green LED's have been investigated, with increasing reverse bias up to -30 V. From spectrum-resolved photoluminescence, we observed region of blueshift and redshift in photoluminescence peak energies. From the energy shift, the strength of piezoelectric field was estimated to be 2.1 ± 0.2 MV/cm. Within our bias range, we observed three orders and one order of magnitude changes in carrier lifetime, for blue and green LED's, respectively. These time-domain results are explained by escape tunneling and thermionic emission, together with carrier recombination which depends on the electron-hole wave function overlap change.

DOI: 10.1103/PhysRevB.66.035334 PACS number(s): 77.65.−j, 78.47.+p, 61.66.−f

I. INTRODUCTION

The application of an external electric field perpendicular to the layers of quantum wells (QW's) significantly changes absorption[1–3] and photoluminescence.[4–8] Absorption coefficient and transition energy variations are explained by quantum confined Stark effect (QCSE) by using either variational calculations[1,9] or Green's function approach.[3] From time-domain studies, carrier lifetime enhancement was observed in the low-field regime, and was attributed to the decreased electron-hole wave function overlap.[4,6] For much higher electric fields, tunneling plays a dominant role on decay rates. In GaAs-based QW systems, various tunneling mechanisms, e.g., escape tunneling through tilted barrier,[6,10] resonant tunneling,[11,12] and phonon-assisted tunneling[13–15] were extensively studied. In addition, thermionic emission for carrier transport in QW's was discussed both in the context of cw transport and photocurrent[16–18] and by the time-resolved measurements.[2]

In the material viewpoint, the potential of group III nitride semiconductors such as GaN and InGaN as optoelectronic devices in the blue and ultraviolet spectral range and high-temperature electronic devices has inspired a tremendous interest in recent research. It is known that huge piezoelectric field (PEF) exists in GaN-based heterostructures with wurtzite structure, which has been studied both theoretically and experimentally.[7,8,19–25] Since the direction of the PEF is opposite to the growth direction,[7,8,20–22] electron and hole wave functions are separated in a QW even in the absence of an external electric field. When the sample is under an increasing reverse bias, which compensates the PEF, the spatial separation of the electron-hole wave functions gradually decreases, which is accompanied by the blueshift of the transition energy. In contrast to the typical case of the QCSE in GaAs-based materials where a redshift is observed with increasing reverse bias,[1,2,4,6] the blueshift in InGaN/GaN QW's as a function of increasing reverse voltage[7,8] and the excitation power[26,27] testified to the existence of the PEF. The previous studies, however, have shown large discrepancy of the PEF strength, scattered from 2.45 MV/cm[20] to less than 1 MV/cm[22] even with similar indium composition of around 15–20%. The increase of photoluminescence (PL) lifetime with continuous increase of well width from 2 to 5.5 nm was explained by PEF-induced electron-hole separation.[20] In the recombination lifetime, carrier localization in InGaN quantum well has been introduced to explain the lifetime dependence on detection photon energy, particularly in structures with relatively large indium composition.[8] In a sample with small indium compositions ($\sim2\%$), it was found that excitons are localized at low temperature but delocalized above ~70 K.[28] Although there are numerous experimental reports on various optical properties in GaN-based heterostructures, exclusive evidence for the influence of applied field on carrier decay mechanisms such as tunneling, thermionic emission, and electron-hole recombination is yet to come. Recently, we reported an unambiguous determination of piezoelectric field and tunneling times in blue light-emitting diode (LED) structures.[29]

In this paper we investigate the effects of the applied field and the PEF on PL transition energies and carrier lifetimes. We analyze physical processes that affect the carrier decay rate in quantum wells subject to a perpendicular electric field, based on simple models. We present results on blue and green InGaN/GaN LED structures which allowed us to better understand the carrier decay mechanisms of thermionic emission, recombination, and tunneling, which are dependent on the barrier height, applied field, and other material parameters. We estimate the piezoelectric field strength by applying large electric field and observing the plateau region in the plot of the PL peak energy vs increasing reverse bias. To exactly determine the applied field in the QW's and barriers, we also performed capacitance-voltage (*C-V*) measurements and estimated depletion layer width which is a main voltage drop region in our sample structures. We have obtained the carrier lifetime in time-resolved PL and pump-probe (PP) measurements, where the external bias was applied in the form of cw or square-function pulse. The PL intensity was found to decrease, and is explained by the leakage of photogenerated carriers. We analyze the spectral and temporal changes based on the variational calculations and the semiclassical tunneling and thermionic emission model.

In Sec. II we describe the details of device structures and

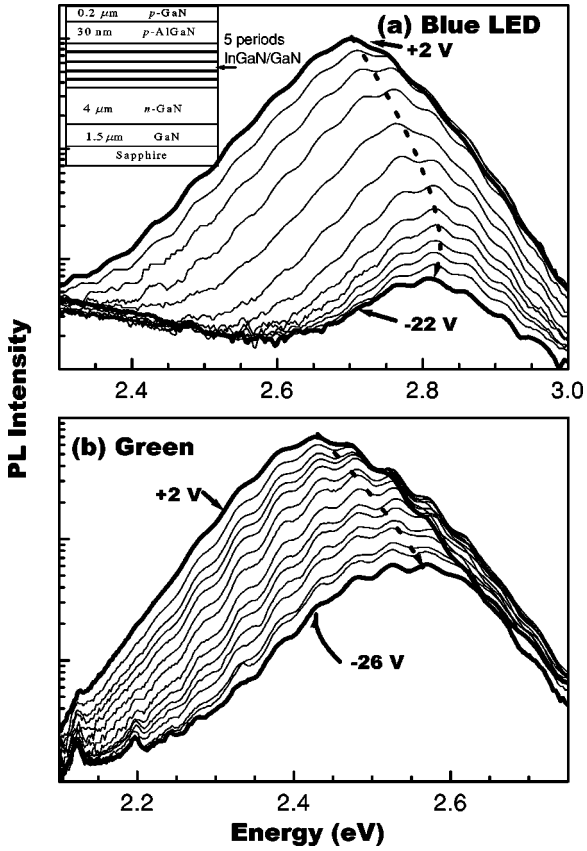

FIG. 1. Room-temperature PL spectra as a function of an external voltage in (a) blue and (b) green LED structures. The inset shows the sample structure, while the AlGaN layer is absent in green LED's.

experiments. The spectral domain results are compared with simple theoretical model to determine the PEF strength and its relation with QCSE in Sec. III. In Sec. IV we discuss the time-domain results for carrier lifetime measurements and the underlying physical processes. Our conclusions are given in Sec. V.

II. SAMPLE STRUCTURE AND EXPERIMENTAL DETAILS

The sample structures are shown schematically in the inset of Fig. 1. Blue (indium composition $\sim$15%) and green LED (indium composition $\sim$20%) structures were grown on a *c*-plane sapphire substrates by metalorganic chemical vapor deposition, where InGaN QW's form the main active region. The following layers were sequentially grown on an undoped 1.5 μm thick GaN layer: 4 μm thick *n*-GaN, five-period $In_xGa_{1-x}N$/GaN (2.2/10 nm for blue LED's, 3.5/24 nm for green LED's), and finally *p*-$Al_{0.1}Ga_{0.9}N$/*p*-GaN (30 nm/0.2 μm for blue LED's) or *p*-GaN (0.2 μm for green LED's). The In mole fraction *x* was estimated by x-ray diffraction which also indicates that the $In_xGa_{1-x}N$ layers are pseudomorpically strained to the underlying *n*-GaN layers.[35,36] Note that we have varied the well and barrier widths simultaneously with the barrier height. The thicknesses of the undoped region were estimated from the cross-sectional image of transmission electron microscopy to be 50 (116) nm for blue (green) LED structures. The Si concentration for *n*-GaN was about 3×10^{18} cm^{-3}, according to SIMS (secondary ion mass spectroscopy) measurements. The Mg concentrations for *p*-GaN and *p*-AlGaN were about 8×10^{19} and 5×10^{19} cm^{-3}, respectively, whereas the hole concentrations of *p*-GaN and *p*-AlGaN were estimated to be about 2×10^{17} and 1×10^{17} cm^{-3}, respectively, by Hall measurements. Only small fraction of the Mg acceptors were activated due to relatively large acceptor binding energy of about 160–290 meV.[37–40] Transparent electrodes were fabricated on top of the *p*-doped layer with an optical window of 330 μm$\times$330 μm. In these structures, the direction of the built-in electric field and reverse applied field are both opposite to that of the PEF.

Time-resolved (TR) and cw PL measurements were carried out varying an external bias from $+2$ to -22 V for blue LED's and $+2$ to -30 V for green LED's, respectively, until the breakdown voltages were reached. A streak camera with 10 ps time resolution was used for TR-PL measurements. To get a better time resolution, femtosecond PP reflectance measurement was carried out over the range from -16 to -30 V in blue LED's, where the pulse duration ($\sim$250 fs) corresponds to the time resolution. Above the static breakdown voltage in blue LED's (~-23 V), an external field was applied in the form of a square-function pulse which was synchronized with the PP detection scheme. The excitation source was a frequency-doubled Ti:sapphire laser, whose energy was fixed at 3.3 (3.15) eV for PL in blue (green) LED's and 3.1 eV for PP measurements. The excitation-power density is estimated to be about 4 kW/cm^2, which corresponds to a carrier density of about the order of 10^{18} cm^{-3}. The background carrier concentration of InGaN is about 10^{18} cm^{-3}, and thus the screening of the electric field in the InGaN layer due to the background carriers is neglected (above 10^{19} cm^{-3}, the screening effect becomes important). All optical experiments as well as *C-V* measurements were done at room temperature.

III. PIEZOELECTRIC FIELD AND QCSE

Figure 1 shows the effect of the applied field on the cw-PL spectra of (a) blue and (b) green LED's. The field in the well was varied by changing the applied voltage V_a from $+2$ V to -22 (-26) V for blue (green) LED's. The oscillations in the spectra of Fig. 1 are modes of the Fabry-Pérot cavity[7,30] whose periodicity is given by $m\lambda=2nl$, where m = mode number, λ = wavelength, n = index of refraction, and l = distance from air-GaN interface to the GaN-sapphire interface ($\sim$5.8 μm in our samples). The relatively large PL width, typical for large In concentrations, is possibly associated with In composition fluctuation[31,32] and the spatial variation of the strain in InGaN layers.[33] The low-energy tail below 2.4 eV in Fig. 1(a) is associated with the well-known yellow luminescence.[34]

The most apparent feature in Fig. 1 is the shift of the PL peak energy with increasing reverse bias. A clear blue shift followed by a redshift is observed in Fig. 1(a) (see the dotted arrow). On the other hand, the PL peak in a green LED is

blueshifted up to -26 V. The blueshift indicates the compensation of the PEF by the applied field, leading to the decrease of the total electric field in the well layers. The redshift, seen in the blue LED, reveals that the net electric field in InGaN is inverted. These effects of energy variations have been explained in terms of the Stark shift of a strongly confined hydrogenic system.[1] As shown in Fig. 1, the PL intensity decreases as the reverse voltage was increased, but the PL of the blue LED decreases at a much faster rate. The faster PL intensity decrease in the blue LED's was accompanied with more dramatic lifetime change, which will be described in the next section.

The PL linewidth was between 136 (147) meV and 145 (180) meV in blue (green) LED's all over the bias range, which was significantly smaller than the difference between the lowest and the second lowest bound state that was estimated to be 430 (520) meV in blue (green) LED's. Hence, we believe that the PL emission originates mainly from the lowest transition. In our QW samples, the exciton binding energy in the absence of any electric field is expected to be more than 40 meV.[24,41] However, with the PEF, the exciton binding energy will be somewhat reduced to be about or less than 30 meV.[41] The exciton binding energy, therefore, is much smaller compared to the separation between the quantum-confined subbands and also the inhomogeneous linewidth broadening in these systems. In contrast to the clear exciton peaks observed in bulk GaN, experimental evidences and theoretical agreements of exciton bands and their variation under the electric field are lacking in InGaN bulk and QW's. In this paper, the variation of Coulomb attraction with respect to the external field is neglected, and the exciton binding energy is assumed to be constant at 30 meV in our calculations.

In order to analyze the PL peak energy under the assumption of no variation in Coulomb interaction between electrons and holes, we solved the Schrödinger equations for the motion perpendicular to the layers (z direction) by using variational calculations. Neglecting the screening effect both by the background carriers and by photoexcited carriers, the net electric field within the wells (barriers) E_w (E_b) was formulated by[7,42]

$$E_w = \frac{V_{\mathrm{bi}} - F_p N_w L_w - V_a}{N_w L_w + N_b L_b + L_d/2} + F_p, \tag{1}$$

$$E_b = \frac{V_{\mathrm{bi}} - F_p N_w L_w - V_a}{N_w L_w + N_b L_b + L_d/2}, \tag{2}$$

where V_{bi}, F_p, and V_a are the built-in potential, the piezoelectric field, and the applied voltage, respectively. $L_w(L_b)$, N_w (N_b), and L_d represent the well (barrier) width, the number of wells (barriers), and the depletion width, respectively. To be self-consistent with the Poisson equation, the electric field in the depletion region was assumed to be linearly varying from zero to a maximum value,[43] which resulted in $L_d/2$ instead of L_d in Eqs. (1) and (2). In Eq. (2) the PEF in GaN barriers was neglected, but the potential drop all across the sample is conditioned to be the same as the built-in potential if there is no externally applied electric field. In order to determine the electric field whose accuracy is important to get the appropriate value of the lowest confined level energy and the corresponding wave function, we need to estimate V_{bi} and L_d. The values of V_{bi} and L_d can be evaluated from Poisson equation only if the donor and acceptor concentrations are known. Based on the carrier concentrations and the particular effective mass values, we estimated the built-in potential to be 3.4 V. However in GaN, the acceptor concentrations are difficult to be exactly determined, since the hole concentrations estimated from Hall measurements can be significantly smaller than the acceptor concentrations due to the relatively large acceptor binding energy. For this reason, the depletion width was obtained from capacitance-voltage (C-V) measurements.[43]

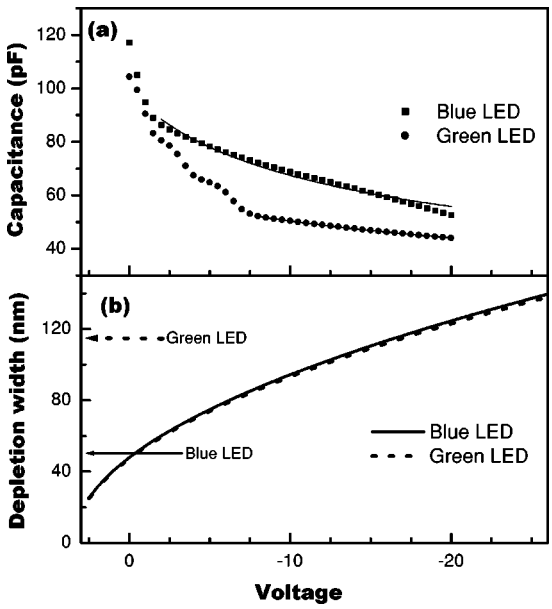

FIG. 2. (a) Capacitance-voltage characteristics at room temperature and (b) depletion widths deduced from the measured capacitance. The horizontal arrows indicate the intrinsic region thicknesses.

Figure 2 shows the results of the C-V measurements and the corresponding depletion width deduced from fitting. Over the bias range from 0 to -20 V under the modulation frequency of 1 MHz, we obtained the data denoted by solid squares for a blue LED and solid circles for a green LED in Fig. 2(a). The bias region with weak oscillatory behavior with steep change of capacitance is not clearly understood but possibly related with charge trapping associated with point defects. It is known that the capacitance associated with the trapping centers depend on the modulation frequency and can be neglected at an infinite frequency limit.[43–45] Ignoring the frequency-dependent terms which are not related with the depletion width estimation, we fitted the data of Fig. 2(a) over the region denoted by the solid lines. Considering the series combination of the capacitances in the intrinsic and doped regions, the capacitance C can be well fitted with the formula

$$C = \left(\frac{1}{C_p} + \frac{1}{C_n} + \frac{1}{C_i} \right)^{-1} = \frac{A \epsilon_s}{N_w L_w + N_b L_b + L_d}, \tag{3}$$

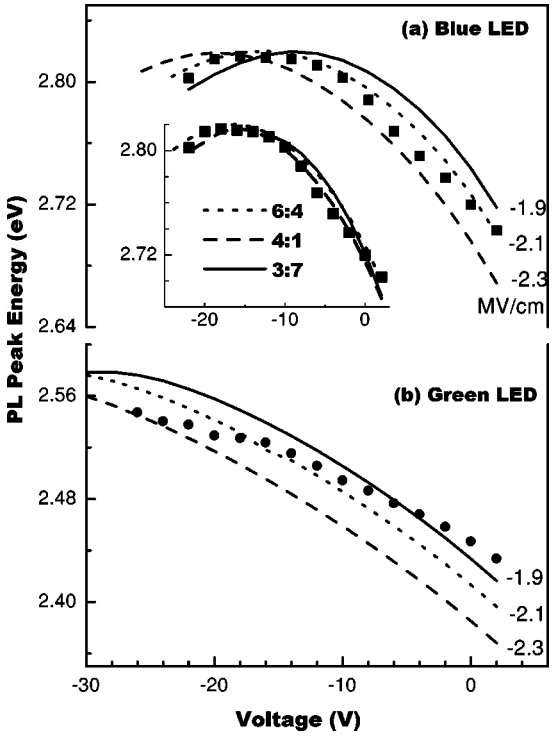

FIG. 3. PL peak energy of the QW's as a function of an external voltage for (a) blue and (b) green LED structures. The scattered curves are experimental data and the curves are from calculations with various piezoelectric field values. The inset shows the PL peak energy with different band offset ratios, setting the piezoelectric field at 2.1 MV/cm.

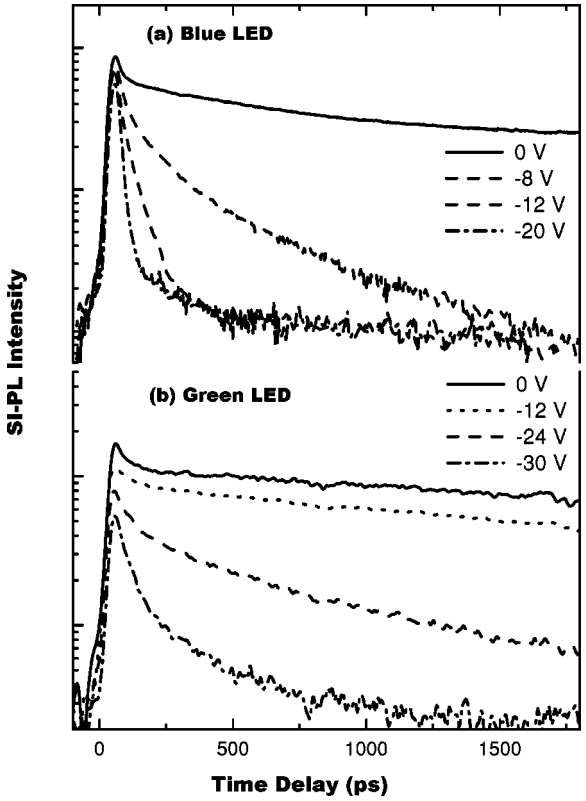

FIG. 4. Spectrally integrated PL traces with increasing reverse bias in (a) blue and (b) green LED structures.

where C_p (C_n) and C_i are the capacitance in the p-doped (n-doped) region and intrinsic region, respectively, with the sample area A and the static dielectric constant ϵ_s. Depletion layer width L_d was simplified as $L_d = \alpha\sqrt{V_{\rm bi} - V_a}$, where α is a fitting parameter. The depletion width thus deduced are shown in Fig. 2(b) for the blue (solid line) and the green LED's (dotted line). The horizontal arrow indicates the intrinsic region thickness.

Following the procedures discussed above, we can compare the PL peak energy traces (scattered curves) with calculations (line curves), as shown in Fig. 3. Here, we used the variational method[9] to get the solutions of Schrödinger equations as we change the value of F_p. The PL peak energies were obtained from Gaussian-fitting after removing the interference fringes. In blue LED data, as can be seen in Fig. 3(a), the most plausible PEF value was -2.1 MV/cm. The inset in Fig. 3(a) shows energy dependence on the band offset ratio between the conduction and valence band, with F_p fixed at -2.1 MV/cm. As we can see in the inset figure, the band offset ratio was not a critical factor and 6:4, 4:1, and even 3:7 result in similar traces as long as the QW bound states exist. In the calculations of Fig. 3, for a convenience' sake, 6:4 ratio was used.

In contrast to the results of the blue LED's, the calculated curves for the green LED's [Fig. 3(b)] exhibit disagreement and show larger energy change than the experimental data. The smaller energy change in the experimental data possibly indicates that the electric field in the green LED's was not fully effective compared to the blue LED's. We cannot explain the main origin for this at the present time, but the screening of the electric field by free and photogenerated carriers,[26] Stokes shifts,[46] and the influence of compositional fluctuations, whose effects are possibly larger in the green LED's with larger well widths and indium compositions to reduce the field-induced energy shift. Further studies on those topics are necessary. Accurate determination of the PEF strength is difficult in the green LED's due to the discrepancy between experiments and calculations and due to the absence of the redshift or plateau region in the plot of PL energy vs voltage, namely, the fact that the PEF is was not fully compensated by the applied field. The bulk $In_xGa_{1-x}N$ energy was assumed to be 2.647 eV (for the blue LED's) and 2.488 eV (for the green LED's) by including the gap fluctuation[46,47] and other material parameters were obtained from Ref. 25.

IV. CARRIER DECAY MECHANISMS

A. Experimental results

Results of the time-resolved PL measurements for the (a) blue and (b) green LED's are shown in Fig. 4. The spectra in Fig. 4 were spectrally integrated except for the scattered laser noise, which was rejected by a grating and slit pair. The decrease of carrier lifetime with increasing reverse biase is readily observed and it is more drastic in the blue LED's even with narrower bias range. These spectrally integrated (SI)-PL traces show biexponential line shapes: (1) in small

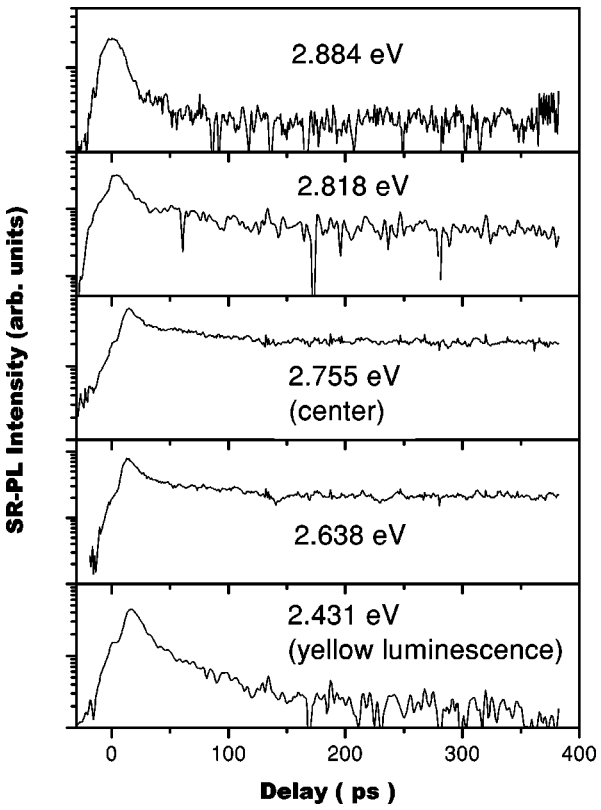

FIG. 5. Time-resolved PL traces at 0 V, with spectral detection window of 40 meV, where the detection center energies are denoted in the figure. The bottom trace is for the low-energy tail associated with the yellow luminescence.

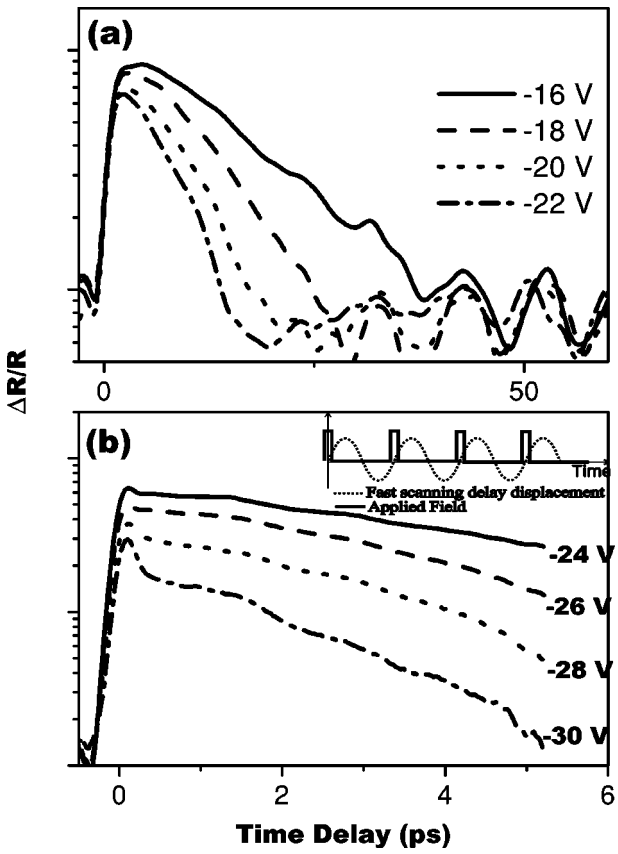

FIG. 6. Differential reflectance spectra with an external voltage from −16 to −30 V. The external field was static for (a) and pulsed for (b). The schematic of the applied field and delay displacement is shown in the inset.

external bias region, the main decay component of the order of ns was mixed with a fast decay component comparable to the time-resolution of the streak camera, (2) in larger external bias, say, −20 V in Fig. 4(a), slower decay components whose decay times were independent of the field followed the main signal. Except for these minor and bias-independent components, lifetime was decreased from 2.5 ns (4 ns) to the resolution limit of 10 ps (280 ps) in the blue (green) LED's over the bias range shown in the figure. The three order of magnitude lifetime change in the blue LED's and one order of change in the green LED's are consistent with the decrease of PL intensity in Fig. 1.

The biexponential behavior mentioned in the previous paragraph has been often observed in InGaN (Refs. 48–50) and can be understood as a results of spectral integration over various components whose decay times are noticeably different from each other in these sample structures.[8,28,50] The fast initial component for small bias is owing to the spectral integration of our signal and corresponds to rapid decay of higher PL energy components as revealed by our spectrum- and time-resolved PL as shown in Fig. 5 for the blue LED. The same is true for the slower component at large bias: these are from the low energy tails of PL (yellow luminescence). In Fig. 5, the SR-PL was measured by a streak-camera together with a spectrometer, where the detection spectral window was fixed at 40 meV with the center energy given in the figure. In addition to the decay time change, the first two traces show somewhat faster rise time than others. The detection energy dependence of decay time is possibly due to the screening of the localized potential[8,28,61] and the piezoelectric potential. Immediately after the excitation whose peak power density can reach up to about 200 MW/cm^2, the photocarrier density in QW's can be sufficient to screen the PEF.[26] With evolving time the screening of the field decreases due to the loss of excess carriers by various decay processes and the carriers are finally in the lowest energy state.[51] The bottom trace in Fig. 5 seems to have different origin with others and corresponds to the yellow luminescence.

In the blue LED samples, the decay trace over −16 V was limited by the instrumental resolution of the streak camera. To overcome this limit in time domain, we performed differential reflectance measurements as a function of probe delay. Figure 6 shows the differential reflectance data for the blue LED samples, where the external voltage was varied from −16 to −30 V. The external voltage was static for Fig. 6(a), but was in the form of square function pulse for Fig. 6(b) to avoid the device breakdown. The experimental scheme is shown in the inset of Fig. 6(b) for the pulsed external bias which was synchronized with the fast scanning delay stage. The fast scanning delay stage with 30 Hz repetition rate generated total time delay of about 30 ps between the pump and probe pulse and 5 ps during the presence of the voltage pulse.

The logarithmic plot of the differential reflectance spectra clearly demonstrates that the differential reflectance decays faster with increasing reverse bias from -16 to -30 V. Note that the probe delay range in Fig. 6(b) is 10 times shorter than Fig. 6(a). In general, the photo-carriers excited by an ultrashort pulse will undergo several scattering and relaxation processes before they again reach a thermal equilibrium. Carrier-carrier scattering is primarily responsible for redistributing the energy within the carriers (typically within hundreds of femtoseconds), leading to thermalized distribution of carriers, at a temperature higher than the lattice temperature. These hot carriers cool down to a lattice temperature through various carrier-phonon interactions.[52] Even at this stage, however, there exist excess carriers which will disappear either by radiative recombination or by other decay dynamics. Regarding the external voltage dependence of the carrier dynamics shown in Fig. 6, we only focus on carrier decay dynamics in this final stage since the initial carrier dynamics typically occur on a much shorter time scale[54] and because it is probably difficult to explain the observed voltage dependence. As we will discuss in the following section, escape tunneling rate is expected to be the most important factor for the carrier decay dynamics under the huge external bias, and thus both the PP and PL lifetimes will be mainly determined by the escape tunneling rate for the high voltage range. For this reason, the PP data are given instead of (or, together with) the PL data only under the large reverse voltage, where PL data cannot give an accurate value due to its relatively poor time resolution. We note here that the decay time of the differential reflectance was found to decrease with increasing excitation energy, i.e., for an excitation energy of 3.3 eV the decay time was shorter than that shown in Fig. 6. The explanation will be given in Sec. IV C, when we discuss photocurrent and photoluminescence. We show the PP data at 3.1 eV in Fig. 6 since it was difficult to obtain the differential reflectance signal with an excitation energy of 2.8 eV near the PL peak energy. In the figure, the oscillations of about 10 ps in Fig. 6(a) and 1.5 ps period in Fig. 6(b), which were not influenced by the external field change, originate from the propagating mode[53] and zone-folded mode of coherent acoustic phonons in these structures.[54]

B. Comparison with simple models

The carrier lifetime keeps decreasing as the PEF is compensated by the reverse bias field. This decreasing carrier lifetime with bias voltage can be induced by an enhanced recombination due to the increased electron-hole wave function overlap and carrier sweep-out such as tunneling and thermionic emission, where each process competes with the others, while the bias dependence of each mechanism is qualitatively the same in strained InGaN QW's. The carrier lifetime τ in a quantum well in an electric field is thus given by the recombination time τ_R, thermionic emission time τ_{TE}, and tunneling time τ_T:

$$1/\tau = 1/\tau_R + 1/\tau_{TE} + 1/\tau_T, \tag{4}$$

where the three mechanisms are assumed to be independent of each other.

To compare the experimental results with theoretical curves, we consider first the simple theoretical model for carrier recombination time. In the one-particle picture

$$\tau_R = \frac{\tau_0}{\left| \int_{-\infty}^{\infty} dz\, \phi_e(z_e)\, \phi_h(z_h) \right|^2}, \tag{5}$$

where $\phi_i(z_i)$ is the wave function with $i=e$ (electron) or h (hole), and τ_0 is the lifetime under flat-band conditions.[6,9] At room temperature the recombination is affected by nonradiative decay channels such as trapping[28] and thermal spread due to the Boltzmann distribution of carriers in the bands.[55] Furthermore, the carrier lifetime in the flat band τ_0 is not known in these strained structures. To focus on the field-dependent effect of recombination, we analyze the recombination based on Eq. (5), setting τ_0 as a fitting parameter.

The thermionic emission and tunneling are sweep-out mechanisms which generate the photocurrent.[2,16,18,56] The thermionic emission lifetime in QW's, derived under the Boltzmann-like carrier statistics and under the assumption that the density of states close to the top of barrier is essentially three dimensional, has the following expression:[16]

$$\tau_{TE} = L_w \sqrt{\frac{2\pi m_i}{k_B T}} \exp\left[\frac{H_i(V_a)}{k_B T}\right], \tag{6}$$

where $H_i(V_a)$ is the bias-dependent effective barrier height over which the carriers must be emitted. Here m_i is the effective mass in the quantum well, T is the temperature. The emission rate against the field is ignored and the barrier height is simplified by $H_i(V_a) = \Delta_i - \varepsilon_i + |eE_w| L_w/2$, where Δ_i is the band discontinuity between the well and barrier material. As the reverse bias cancels out the PEF, the ε_i increases while E_w decreases to lower the $H_i(V_a)$, and thus the emission rate increases until the potential in QW's become flat. Due to the strong dependence of τ_{TE} on barrier height, holes can be emitted faster than electrons when we use the values between 6:4 (Ref. 34) and 4:1 (Ref. 57) as a ratio of conduction and valence band discontinuities, even though the effective mass is larger for holes. Lower indium composition also leads to the faster emission rates by reducing Δ_i. In our calculations, the presence of the $Al_{0.1}Ga_{0.9}N$ layer in blue LED's was neglected to avoid the further complexity of Eq. (6) but it can somewhat suppress the transport of holes under the reverse external voltage, especially for the topmost one among the five QW's. Hence, the thermionic emission which is dominated by the holes are possibly overestimated in our blue LED's.

Tunneling rate is also a function of the field-dependent barrier height but the effective mass is another important parameter. The tunneling time in the Wentzel-Kramers-Brillouin (WKB) approximation[6,10,58] is given by the product of the barrier collision frequency and the tunneling probability

$$\tau_T = \frac{\hbar \pi}{\varepsilon_i} \exp\left[\int_0^W 2 \sqrt{\frac{2m_i}{\hbar^2} [H_i(V_a) - eE_b z]}\, dz \right], \tag{7}$$

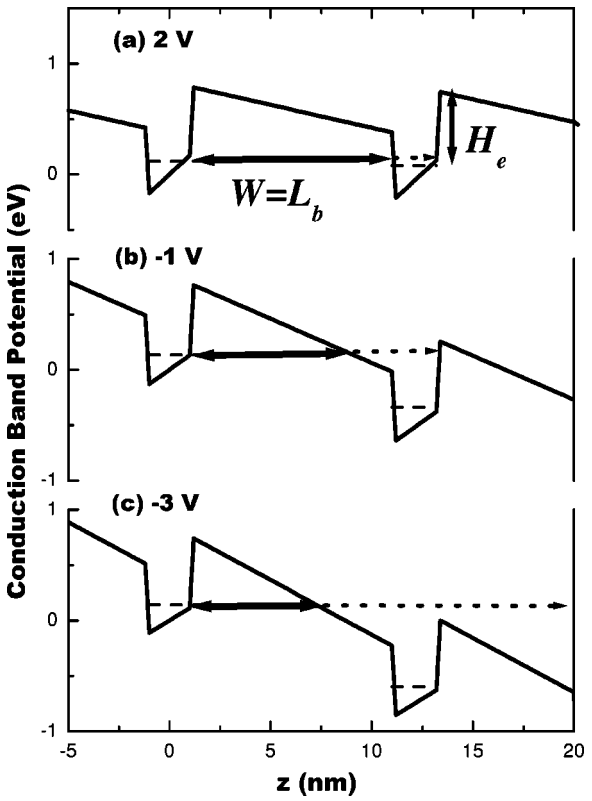

FIG. 7. Schematic of conduction band alignment with the external voltages of (a) 2 V, (b) -1 V, and (c) -3 V. W and H_e are the effective tunneling barrier width and barrier height, respectively. As seen in Fig. (c), only single barrier tunneling occurs for an external voltage less than -3 V.

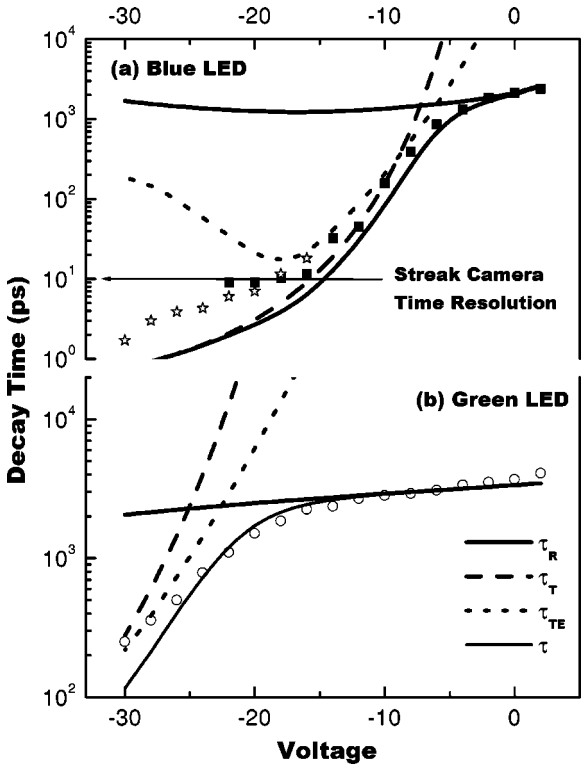

FIG. 8. Carrier lifetime as a function of an external voltage for (a) blue and (b) green LED structures. The scattered data are experimental and the curves are from calculations. The open stars in (a) are obtained from the pump-probe reflectivity measurements. The carrier lifetime τ was obtained taking into account recombination time τ_R, tunneling time τ_T, and thermionic emission time τ_{TE}.

where the integration is carried over the effective barrier thickness W in case of single barrier transmission. $H_i(V_a) - eE_b z$ is the barrier height as the carriers go through the GaN region. Electrons have much faster tunneling rate than holes due to their five times lighter effective mass[25] and only the electron tunneling was included in our calculations, where the effective electon mass m_e has a value of $0.2m_0$ both in the well and barrier.[25]

The effective barrier thickness W is a function of the external bias and determined by

$$W = L_b \quad \text{for} \quad \frac{H_i(V_a)}{eE_b} \geqslant L_b, \tag{8a}$$

$$W = \frac{H_i(V_a)}{eE_b} \quad \text{for} \quad W < L_b. \tag{8b}$$

Figure 7 shows the potential shape (solid lines), the confined energy in the well ε_e (dotted line), and the corresponding barrier thickeness W (thick arrow) for the indicated external voltage in the blue LED samples. In Fig. 7(a) the value of W is equal to the actual barrier width, otherwise, we determine W from Eq. (8b). The samples have five QW's, in contrast to the simplification of single barrier used in Eq. (7), where the multiple barrier transmission could occur over the range from $+2$ to -2 V (note the dotted arrows in Fig. 7). The tunneling in this range of multiple barrier transmission was negligibly slower than other decay mechanisms in both sample structures. In addition, Eq. (8b) is always satisfied for the condition of single barrier transmission in our structures. Thus, in our calculation, tunneling can practically contribute to the total carrier lifetime only for the case of Fig. 7(c) with single barrier and W smaller than L_b.

Over the bias range used here, resonant tunneling[11,12] does not play an important role since the lowest energy levels in adjacent wells are not aligned to be the same. The interwell energy alignment for resonant tunneling is expected with voltage larger than $+2$ V, but the relatively large barrier width makes it difficult to observe an evidence of resonant tunneling. Tunneling assisted by thermal phonon emission which has been observed in GaAs QW (Ref. 13) and InGaAs QW (Ref. 14) could be also neglected due to the large barrier widths in our samples. In addition, the photogenerated carriers which are emitted out of the quantum wells to the continuum of states above the potential barriers can be recaptured by one of the wells after traveling a mean free path.[59] Further experimental and theoretical investigations of those resonant tunneling, phonon-assisted tunneling, and recapturing process would lead to better understanding of the fundamental aspects of these structures. The tunneling time becomes faster as the barrier thickness W is decreased by the applied voltage V_a. In the blue LED samples, W starts with 10 nm (at $+2$ V) and reach 1.7 nm (at -30 V).

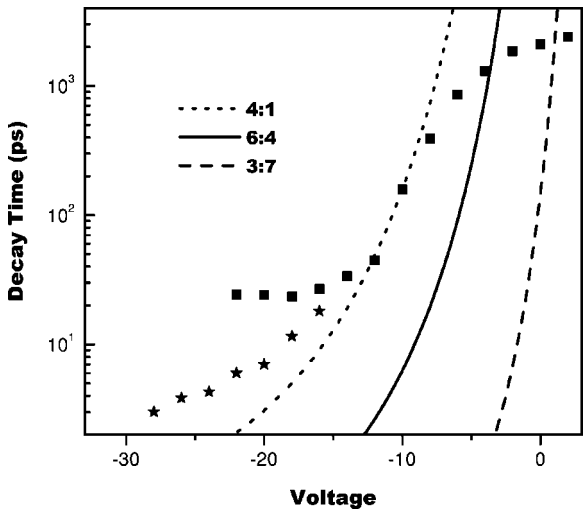

FIG. 9. Carrier lifetime as a function of an external voltage for (a) blue and (b) green LED structures. The scattered data are experimental and the curves are from calculations. The open stars in (a) are obtained from the pump-probe reflectivity measurements. The carrier lifetime τ was obtained taking into account recombination time τ_R, tunneling time τ_T, and thermionic emission time τ_{TE}.

Figure 8 summarizes the calculated values of τ_R (ashy solid curves), τ_T (dashed), τ_{TE} (dotted), and τ (solid) as a function of field strength. The scattered data are from PL experiments except for the PP data denoted by hollow stars. By adding up the three contributions described above, we can achieve agreements between experimental and calculated values of τ. The carrier lifetime τ is mainly determined by the smallest value among τ_R, τ_T, and τ_{TE} in Eq. (4). The measured lifetime rapidly decreases with increasing reverse bias after a certain onset voltage is reached and, then the decreasing trend becomes somewhat slower near the largest reverse bias. The comparison of the data for the two structures with different barrier height and thickness demonstrates that the onset voltage of carrier sweep-out shifts to a larger external voltage for the green LED's. In the blue LED's the change of carrier decay time by three orders of magnitude is mostly due to the escape tunneling. On the other hand, sweep-out processes were less important for determining τ in the green LED's, which is expected due to the larger barrier height and barrier width, hence, τ was influenced by τ_R for a broader bias range. The well widths which were smaller than (for the blue LED's) or comparable to (for the green LED's) bulk exciton Bohr radius ($\sim$3.4 nm) keep the τ_R within a limited change due to the slight wave function overlap change. When we compare the sweep-out mechanisms of τ_T and τ_{TE}, we find that thermionic emission is effective for relatively small reverse bias region.

In calculating τ_T and τ_{TE} the band offset ratio was a major parameter, as shown in Fig. 9. Figure 9 shows the τ_T for several band offset ratios in blue LED's, where 4:1 ratio gives the best fit. The band offset ratio of 4:1 has been used for the calculations in Fig. 8. However, the quantitative agreement which is realized in Fig. 8 and Fig. 9 does not necessarily imply that we determined an accurate value of the band offset ratio in the strained InGaN QW's because (1) we are neglecting the compositional and potential fluctuation[60,61] and corresponding carrier localizations,[8,57,62] (2) we assumed that the electric field in the wells and barriers are spatially constant, an oversimplification in certain cases, and (3) we neglected the defects and impurities at the well interfaces which can act as carrier trapping centers.

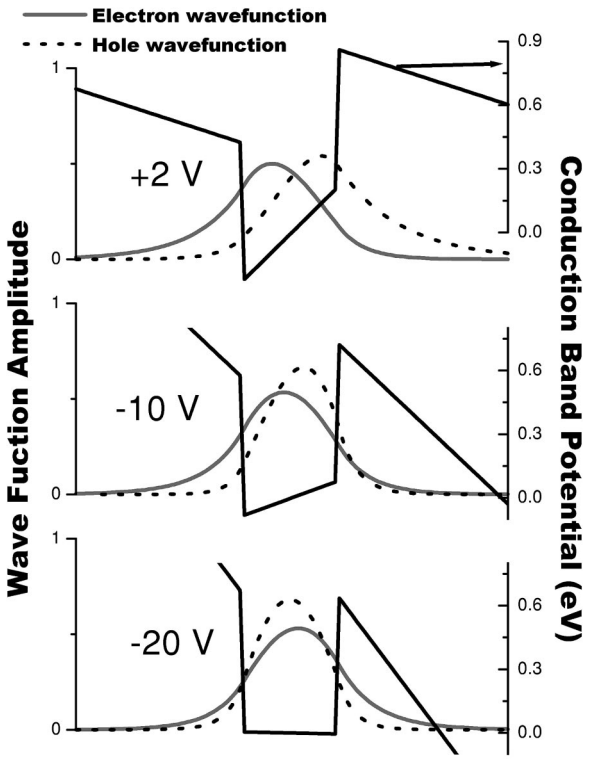

FIG. 10. Carrier lifetime as a function of an external voltage for (a) blue and (b) green LED structures. The scattered data are experimental and the curves are from calculations. The open stars in (a) are obtained from the pump-probe reflectivity measurements. The carrier lifetime τ was obtained taking into account recombination time τ_R, tunneling time τ_T, and thermionic emission time τ_{TE}.

The relatively large discrepancy between experiments and calculations in the PP measurement range is not yet clearly understood. The discrepancy is possibly associated with the oversimplification in the potential profile and the errors in material parameters, including the depletion width, which was obtained from fitting over only small bias range. In addition, intraband redistribution process of carriers may influence the PP signal, and thus the PP decay time is not proportional to the total carrier concentration near zero-time delay.

C. Photocurrent and photoluminescence

In Fig. 10, electron and hole wave functions are plottted for $+2$, -10, and -20 V, as well as the conduction band potential. At $+2$ V, the electron and hole wave functions are pushed away to the opposite sides. The wave fuction separation effect is less pronounced at -10 V, and finally exchange the position with a penetration of the electon wave fuction tail through the barrier at -20 V. The hole wave fuction shift is more pronounced than the electron shift be-

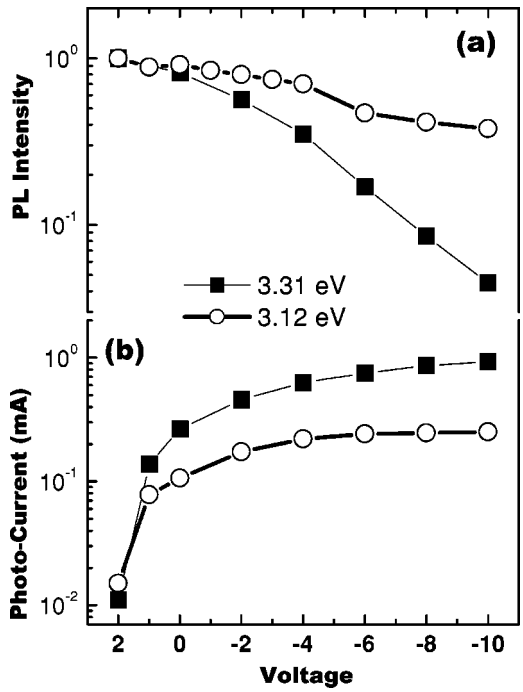

FIG. 11. (a) PL intensity and (b) photocurrent as a function of an external voltage with laser excitation energies of 3.31 eV (filled square) and 3.12 eV (open circle).

cause the barrier height in the valence band is smaller and the effective mass is larger.[9] The overlap integral, influenced by the spatial separation, increases up to flat QW region, which may result in an increase of the PL intensity if all the carriers were to decay by radiative recombination. On the other hand, the carrier sweep-out processes may cause the leakage of photogenerated carriers through or above the GaN barriers. It is thus interesting to examine the PL intensity change in the small bias region where the sweep-out process is less effective.

In Fig. 11 we show (a) PL intensity and (b) photocurrent as a function of the applied voltage at an excitation energy of 3.31 eV (filled squares) and 3.12 eV (open circles) in the blue LED's. The PL intensity traces in Fig. 11(a) are normalized to have the same maximum value. The direction of the photocurrent (the current change with and without laser excitation) was opposite to that of the piezoelectric field. As the reverse bias is increased (i.e., the PEF is compensated by the external electric field) the continual decrease of the PL intensity is accompanied by an increase of photocurrent. This result provides an evidence that the observed variation of the PL intensity with the increasing reverse bias is not significantly dependent on the electron-hole wave function overlap, but dependent on the carrier sweep-out rates. From the comparison of Figs. 11(a) and 11(b), we can conclude that the rate of decrease in PL intensity is mainly determined by the amount of leakage photocurrent; the smaller current increase for 3.12 eV in Fig. 11(b) corresponds to the slower decrease of the PL intensity in (a).

The photocurrent in the low-field region where tunneling is less effective can be attributed to the thermionic emission[2,16,61] and possibly some background nonradiative transitions via defects and impurities. In the region of higher fields, tunneling out of the quantum wells dominates the photocurrent process.[6,56,63] The larger photocurrent with higher laser energy as shown in Fig. 11(b), is possibly due to the increased absorption coefficient and the corresponding increase of the photoexcited carrier density. Another point to address is that the tunneling lifetime in Fig. 8 is estimated for the electrons in the lowest energy level. In our experiments, however, the excitation energy is much larger than the PL energy. When we apply the semiclassical tunneling model to the carriers with larger energy such as 3.3 eV, tunneling is much more efficient, which can be similar to or even faster than the fast initial carrier cooling time of about 500 fs which was measured in InGaN bulk when the excitation energy was similar to our case.[64] Such tunneling of carriers which occur before the carriers relax to sufficiently lower energy states can also contribute to the photocurrent which depends on the excitation energy. The PL intensities and photocurrents in the green LED's change at a similar but reduced rates, indicating that the effects of the electric field on the carrier leakage involved in the PL intensity are comparable for both blue and green LED's.

V. CONCLUSION

The carrier decay dynamics of InGaN/GaN QW's, under an external electric field which compensates the PEF, have been investigated both in spectrum and time domains. The PEF strength was estimated to be about 2.1 ± 0.2 MV/cm by observing the plateau region and the redshift in the plot of the PL energy with increasing reverse voltage. We have observed three orders and one order of magnitude change in carrier lifetime of the blue and green LED's, respectively, as a function of reverse bias. At low fields, the main decay channels are thermionic emission and carrier recombination. For higher fields, tunneling of carriers through the tilted barriers becomes dominant. We have also shown that the PL intensity decrease is associated with the leakage of the carriers through the barriers. Our results imply that the response time of GaN-based optoelectronic devices can be comparable or even faster than that of GaAs QW.[65]

ACKNOWLEDGMENTS

This work was supported by Korea Research Foundation Grant (Grant No. KRF-2000-015-DP0137). The samples used in this work were provided from Samsung electronics.

*Electronic address: esoh@phya.snu.ac.kr

[1] D.A.B. Miller, D.S. Chemla, T.C. Damen, A.C. Gossard, W. Wiegmann, T.H. Wood, and C.A. Burrus, Phys. Rev. Lett. **53**, 2173 (1984); Phys. Rev. B **32**, 1043 (1985).

[2] A.M. Fox, D.A.B. Miller, G. Livescu, J.E. Cunningham, and W.Y. Jan, IEEE J. Quantum Electron. **27**, 2281 (1991).

[3] S.L. Chuang, S. Schimitt-Rink, D.A.B. Miller, and D.S. Chemla, Phys. Rev. B **43**, 1500 (1991).

[4] H.-J. Polland, L. Schultheis, J. Kuhl, E.O. Göbel, and C.W. Tu, Phys. Rev. Lett. **55**, 2610 (1985).
[5] E.E. Mendez, G. Bastard, L.L. Chang, L. Esaki, H. Morkoc, and R. Fischer, Phys. Rev. B **26**, 7101 (1982).
[6] K. Köhler, H.-J. Polland, L. Schultheis, and C.W. Tu, Phys. Rev. B **38**, 5496 (1988).
[7] T. Takeuchi, C. Wetzel, S. Yamaguchi, H. Sakai, H. Amano, I. Akasaki, Y. Kaneko, S. Nakagawa, Y. Yamaoka, and N. Yamada, Appl. Phys. Lett. **73**, 1691 (1998).
[8] S.F. Chichibu, T. Azuhata, T. Sota, T. Mukai, and S. Nakamura, J. Appl. Phys. **88**, 5153 (2000), and references quoted therein.
[9] G. Bastard, E.E. Mendez, L.L. Chang, and L. Esaki, Phys. Rev. B **28**, 3241 (1983).
[10] T.B. Norris, X.J. Song, W.J. Schaff, L.F. Eastman, G. Wicks, and G.A. Mourou, Appl. Phys. Lett. **54**, 60 (1989).
[11] K. Leo, J. Shah, E.O. Göbel, T.C. Damen, Köhler , and P. Ganser, Appl. Phys. Lett. **56**, 2031 (1990).
[12] D.Y. Oberli, J. Shah, T.C. Damen, C.W. Tu, T.Y. Chang, D.A.B. Miller, J.E. Henry, R.F. Kopf, N. Sauer, and A.E. DiGiovanni, Phys. Rev. B **40**, 3028 (1989).
[13] D.Y. Oberli, J. Shah, T.C. Damen, J.M. Kuo, J.E. Henry, J. Lary, and S.M. Goodnick, Appl. Phys. Lett. **56**, 1239 (1990).
[14] M.G. Shorthose, J.F. Ryan, and A. Moseley, Solid State Electron **32**, 1449 (1989).
[15] A. Larsson, P.A. Andrekson, S.T. Eng, and A. Yariv, IEEE J. Quantum Electron. **24**, 787 (1988).
[16] H. Schneider and K.v. Klitzing, Phys. Rev. B **38**, 6160 (1988).
[17] R.T. Collins, K.V. Klitzing, and K. Ploog, Appl. Phys. Lett. **49**, 406 (1986).
[18] M. Dutta, K.K. Choi, and P.G. Newman, Appl. Phys. Lett. **55**, 2429 (1989).
[19] F. Bernardini, V. Fiorentini, and D. Vanderbilt, Phys. Rev. B **56**, R10 024 (1997).
[20] P. Lefebvre, A. Morel, M. Gallart, T. Taliercio, J. Allgre, B. Gil, H. Mathieu, B. Damilano, N. Grandjean, and J. Massies, Appl. Phys. Lett. **78**, 1252 (2001).
[21] J.S. Im, H. Kollmer, J. Off, A. Sohmer, F. Scholz, and A. Hangleiter, Phys. Rev. B **57**, R9435 (1998).
[22] C. Wetzel, T. Takeuchi, H. Amano, and I. Akasaki, Phys. Rev. B **61**, 2159 (2000).
[23] H. Kollmer, J.S. Im, S. Heppel, J. Off, F. Scholz, and A. Hangleiter, Appl. Phys. Lett. **74**, 82 (1999).
[24] S.F. Chichibu, A.C. Abare, M.S. Minsky, S. Keller, S.B. Fleichser, J.E. Bowers, E. Hu, U.K. Mishra, L.A. Coldren, S.P. DenBarrs, and T. Sota, Appl. Phys. Lett. **73**, 2006 (1998).
[25] T. Takeuchi, S. Sota, M. Katsuragawa, M. Komori, H. Takeuchi, H. Amano, and I. Akasaki, Jpn. J. Appl. Phys., Part 2 **36**, L382 (1997).
[26] P. Riblet, H. Hirayama, A. Kinoshita, A. Hirata, T. Sugano, and Y. Aoyagi, Appl. Phys. Lett. **75**, 2241 (1999).
[27] T. Wang, D. Nakagawa, J. Wang, T. Sugahara, and S. Sakai, Appl. Phys. Lett. **73**, 3571 (1998).
[28] Y. Narukawa, S. Saijou, Y. Kawakami, S. Fujita, T. Mukai, and S. Nakamura, Appl. Phys. Lett. **74**, 558 (1999).
[29] Y.D. Jho, J.S. Yahng, E. Oh, and D.S. Kim, Appl. Phys. Lett. **79**, 1130 (2001).
[30] S. Chichibu, T. Azuhata, T. Sota, and S. Nakamura, Appl. Phys. Lett. **69**, 4188 (1996).
[31] S. Chichibu, T. Azuhata, T. Sota, and S. Nakamura, Appl. Phys. Lett. **70**, 2822 (1997).
[32] E. Oh, M.H. Lee, K.J. Kim, M.Y. Ryu, J.H. Song, S.W. Park, P.W. Yu, H. Park, and Y. Park, J. Appl. Phys. **89**, 2839 (2001).
[33] K.P. O'Donnell, T. Breikopf, H. Kalt, W. Van der Stricht, I. Moerman, P. Demeester, and P.G. Middleton, Appl. Phys. Lett. **70**, 1843 (1997).
[34] Ch. Manz, M. Kunzer, H. Obloh, A. Ramakrishnan, and U. Kaufmann, Appl. Phys. Lett. **74**, 3993 (1999).
[35] T. Takeuchi, H. Takeuchi, S. Sota, H. Sakai, H. Amano, and I. Akasaki, Jpn. J. Appl. Phys., Part 2 **36**, L177 (1997).
[36] J. Wagner, A. Ramakrishnan, D. Behr, M. Maier, N. Herres, M. Kunzer, H. Obloh, and K.-H. Bachem, MRS Internet J. Nitride Semicond. Res. **4S1**, G2.8 (1999).
[37] H. Amano, M. Kito, K. Hiramatsu, and I. Akasaki, Jpn. J. Appl. Phys., Part 2, **28**, L2112 (1999).
[38] M. Ilegems and R. Dingle, J. Appl. Phys. **44**, 4234 (1973).
[39] M. Smith, G.D. Chen, J.Y. Lin, H.X. Jiang, A. Salvador, B.N. Sverdlov, A. Botchkarev, H. Morkoc, and B. Goldenberg, Appl. Phys. Lett. **68**, 1883 (1996).
[40] T. Tanaka, A. Watanabe, A. Amano, Y. Kobayashi, I. Akasaki, S. Yamazaki, and M. Koike, Appl. Phys. Lett. **65**, 593 (1994).
[41] G. Traetta, R. Cingolani, A.D. Carlo, F.D. Sala, and P. Lugli, Appl. Phys. Lett. **76**, 1042 (2000).
[42] J.P.R. David, T.E. Sale, A.S. Pabla, P.J. Rodríguez-Gironés, J. Woodhead, R. Grey, G.J. Rees, P.N. Robson, M.S. Skolnick, and R.A. Hogg, Appl. Phys. Lett. **68**, 820 (1996).
[43] S.M Sze, in *Physics of Semiconductor Devices*, 2nd ed. (Wiley, New York, 1981), and references therein.
[44] W. Schockley and G.L. Pearson, Phys. Rev. **74**, 232 (1948).
[45] Y. Wada and K. Wada, J. Vac. Sci. Technol. B **12**, 3084 (1994).
[46] S.F. Chichibu, A.C. Abare, M.S. Minsky, S. Keller, S.B. Fleischer, J.E. Bowers, E. Hu, U.K. Mishra, L.A. Coldren, S.P. DenBaars, and T. Sota, Appl. Phys. Lett. **73**, 2006 (1998).
[47] L.K. Teles, J. Furthmüller, L.M.R. Scolfaro, J.R. Leite, and F. Bechstedt, Phys. Rev. B **63**, 085204 (2001).
[48] C.I. Harris, B. Monemar, H. Amano, and I. Akasaki, Appl. Phys. Lett. **67**, 840 (1995).
[49] C.K. Sun, S. Keller, G. Wang, M.S. Minsky, J.E. Bowers, and S.P. DenBaars, Appl. Phys. Lett. **69**, 1936 (1996).
[50] M. Pophristic, F.H. Long, C. Tran, I.T. Ferguson, and R.F. Kalicek, Jr., Appl. Phys. Lett. **73**, 3550 (1998).
[51] A. Hangleiter, J.S. Im, H. Kollmer, S. Heppel, J. Off, and F. Scholz, MRS Internet J. Nitride Semicond. Res. **3**, 15 (1998).
[52] J. Shah, *Ultrafast Spectroscopy of Semiconductors and Semiconductor Nanostrucutures* (Springer-Verlag, Berlin 1996), Vol. 115, and references therein.
[53] J.S. Yhang, Y.D. Jho, E. Oh, D.S. Kim, G.D. Sanders, and C.J. Stanton, Appl. Phys. Lett. **80**, 4723 (2002).
[54] C.K. Sun, J.C. Liang, and X.Y. Yu, Phys. Rev. Lett. **84**, 179 (2000).
[55] T. Matsusue and H. Sakaki, Appl. Phys. Lett. **50**, 1429 (1987).
[56] Y. Horikoshi, A. Fischer, and K. Ploog, Phys. Rev. B **31**, 7859 (1985).
[57] T. Deguchi, A. Shikanai, T. Sota, S. Chichibu, and S. Nakamura, Appl. Phys. Lett. **72**, 3329 (1998).
[58] L.D. Landau and E.M. Lifshitz, *Quantum Mechanics, Nonrelativistic Theory*, 3rd ed. (Pergamon, New York, 1977), pp. 178–181.
[59] J.F. Ryan, R.A. Taylor, A.J. Turberfield, A. Maciel, J.M. Worlock,

A.C. Gossard, and W. Wiegmann, Phys. Rev. Lett. **53**, 1841 (1984).
[60] W. Shan, J.J. Song, Z.C. Feng, M. Schurman, and R.A. Stall, Appl. Phys. Lett. **69**, 3315 (1996).
[61] Y.-H. Cho, G.H. Gainer, A.J. Fischer, J.J. Song, S. Keller, U.K. Mishra, and S.P. DenBaars, Appl. Phys. Lett. **73**, 1370 (1998).
[62] Lin-Wang Wang, Phys. Rev. B **63**, 245107 (2001).
[63] L. Viña, R.T. Collins, E.E. Mendez, and W.I. Wang, Phys. Rev. B **33**, R5939 (1986).
[64] C.K. Sun, F. Vallée, S. Keller, J.E. Bowers, and S.P. DenBaars, Appl. Phys. Lett. **70**, 2004 (1997).
[65] G.D. Boyd, A.M. Fox, D.A.B. Miller, L.M.F. Chirovsky, L.A. D'Asaro, J.M. Kuo, R.F. Kopf, and A.L. Lentine, Appl. Phys. Lett. **57**, 1843 (1990).